DEPARTMENT OF PHYSICS
UNIVERSITY OF JYVÄSKYLÄ
RESEARCH REPORT No. 5/2004

PARTITIONING OF PARAMETER SPACES OF PHYSICAL MODELS

BY

JUHANI HÄMÄLÄINEN

Academic Dissertation
for the Degree of
Doctor of Philosophy

To be presented, by permission of the
Faculty of Mathematics and Science
of the University of Jyväskylä,
for public examination in Auditorium FYS-1 of the
University of Jyväskylä on October 30, 2004
at 12 o'clock noon

Jyväskylä
October 2004

ISBN 978-951-39-3154-4
URN:ISBN:978-951-39-3154-4

Preface

The work reviewed in this Thesis has been carried out at the Finnish Defence Forces Technical Research Centre (PvTT), the Swedish Defence Research Agency (FOI) and the Department of Physics in University of Jyväskylä (JYFL) during the years 1999-2004. I would like to express my gratitude to my supervisors and collaborators Dr. Juha Merikoski, Dr. Matias Aunola, Dr. Kari Hirvi, Dr. Mats Bäckström, Mr. Seismo Malm, Mr. Hannu Rajaniemi, Mr. Sami Helle and Mr. Petri Järviö. The additional comments from the readers of the Thesis, Prof. Jan Carlsson and Prof. Lauri Kettunen, and many interesting discussions with colleagues at PvTT, FOI and JYFL are acknowledged. Working conditions and support from my employer PvTT have been excellent. In particular, I would like to thank Research manager Seppo Härkönen. I wish to thank my friends, especially, Jussi Maunuksela, Marko Rasi, Pertti Ahonen, Mika Latva-Kokko and Timo Latva-Pukkila. Finally, I thank my Mother for supporting me through difficult times. This Thesis is dedicated to cycling and cross-country skiing.

Riihimäki, October 2004
Juhani Hämäläinen

Abstract

Hämäläinen, Juhani
Partitioning of Parameter Spaces of Physical Models
Jyväskylä: University of Jyväskylä, 2004.
(Research report/Department of Physics, University of Jyväskylä,
ISSN 0075-465X; 5/2004)
ISBN 951-39-1959-5
Diss.

The aim of this Thesis has been to introduce tools for describing computer simulations in terms of physical and simulation parameters. In practice, we examine the general properties and features of the solutions with respect to the parameters. The developed tools are applied to electromagnetic compatibility problems, particularly determination of shielding effectiveness of rectangular enclosures. Case studies clearly show that the modelled structures, for instance enclosures like common personal computers, cannot provide shielding over a wide range of frequencies of electromagnetic radiation. This approach can be generalised to deal with other parametrised physical problems. The shielding properties are also examined by comparing electric field histograms inside the enclosure.

Keywords: EMC, partitioning, parameter space, shielding effectiveness, statistical electromagnetics

Author's address Juhani Hämäläinen
PvTT
Riihimäki
Finland

Supervisors Docent Juha Merikoski
Department of Physics
University of Jyväskyä
Finland

Docent Matias Aunola
PvTT
Riihimäki
Finland

Dr. Kari Hirvi
Elesco Oy
Espoo
Finland

Reviewers Professor Jan Carlsson
EMC Department
SP Swedish National Testing and Research Institute Electronics - EMC
Borås
Sweden

Professor Lauri Kettunen
Department of Electrical Engineering
Tampere University of Technology
Tampere
Finland

Opponent Professor Ari Sihvola
Electromagnetics Laboratory
Helsinki University of Technology
Espoo
Finland

List of publications

I J. S. Hämäläinen, H. J. Rajaniemi and K. P. Hirvi, *Using Mathematical Models to Cope with Complex Computer Simulations*, IEEE Computing in Science and Engineering, Vol. 4, No. 1, 2002, pp. 64-72.

II J. S. Hämäläinen, P. S. Järviö and S. R. Malm, *Novel description of a numerical EMC problem*, Proceedings of EMC Europe 2002, 9–13 September 2002, Sorrento, Italy, pp. 591-594.

III J. S. Hämäläinen, M. Aunola and S. R. Malm, *Exploring the overall behaviour of solutions of recursive computational models*, to appear in COMPEL, The International Journal for Computation and Mathematics in Electrical and Electronic Engineering, 2005.

IV S. R. Malm and J. S. Hämäläinen, *Grouping the distributions of electric field amplitudes*, Proceedings of the 2003 IEEE International Symposium on Electromagnetic Compatibility, Istanbul, 2003.

V S. R. Malm, J. S. Hämäläinen and S. A. Helle, *Determination of the optimal measurement parameters from simulations*, in Electrical engineering and electromagnetics VI, edited by C. A. Brebbia and D. Poljak, WIT Press, 2003, pp. 293-302.

VI J. S. Hämäläinen, *Are shielding properties of the cavity readable in histograms of electric field amplitudes - to scale or not to scale histograms*, to appear in IEE Proceedings - Science, Measurement and Technology, 2004.

VII J. S. Hämäläinen and J. Merikoski, *Stochastic kinetics with wave nature*, Modern Physics Letters B, Vol. 17, No. 17, 2003, pp. 929-933.

The author of this Thesis has written Papers II, IV, V and VI. The author has written the first draft versions of Papers III and VII and participated in writing the Paper I. Simulations of Papers I-V have been done in co-operation of the

authors. The author has introduced most of the methodology and performed the result analysis of papers I-VI. The author has proposed the Lorentz invariance study in Paper VII.

Contents

Chapter 1

Introduction

In sciences, one of the fastest growing areas during the past twenty years has been computer-based numerical modelling. This is due to increase in computational power as well as various and expanding needs to model complex systems within industry and scientific community. Usually, a simulation model of an industrial application is solved using commercial software packages. Often, the models are idealised and many details are missing, sometimes on purpose. A computer simulation can be either a massive computational problem of solving a set of equations or modelling of a physical process using advanced computational techniques. Invariably, the simulation procedure consists of a model implementation, a solving procedure, and post-processing of the data. In this Thesis, an idealised computer simulation will be interpreted as a mapping from input and implementation parameters to solutions. Such an explicit description is not widely used, but actually it provides a tool to compare solutions and to search for optimal parameters for a specific need. It also enables us to interprete and visualise the overall behaviour of the solutions for the given problem. The meaning of thus clarified results can then be transmitted to non-specialists too.

This Thesis is a review of computational methods, theoretical ideas and their applications as presented in the appended articles. We shall concentrate on recursive computer simulations. We classify the solutions according a cost function, which we shall call a measure of merit (mom). The idea is to group the solutions and, eventually, the parameters with respect to the values of mom. We use the obtained grouping to examine the overall behaviour of the models. We title this approach as "partitioning of the parameter space". To our best knowledge, such an interpretation has not been used to describe and classify computer simulations themselves, not just the final data. We should note here,

that partitioning has been studied in various contexts in pattern recognition, where large data sets are classified into different subsets with respect to data features [1, 2]. In pattern analysis, algorithms can have a learning property as in the case of self-organising maps [3], or they can be based on fuzzy logic [4]. Various methods have been recently reviewed in Ref. [5]. In supervised learning, the examples of the data contain both input and output values. When the task is to understand the process which generated the data, but no outputs are given, learning is unsupervised.

Let us consider the solutions of a recursive numerical model. We aim at a description that provides an efficient way to obtain insight in the behaviour of the solutions. We achieve this by solving the model with selected input parameters and by comparing the solutions as follows. A solution is characterised in terms of the values of the measure of merit. The effects due to the computational accuracy and the technical implementation of the model are taken into account by expanding the parameter space by a cartesian product with an implementation space. For recursive simulations, the implementation can be taken as the recursive order of simulation. The "convergence" of the simulation is studied by comparing the partitionings obtained by successive implementations and different moms are compared by using respective partitionings.

The application part of the Thesis is devoted to electromagnetic compatibility (EMC) problems. We begin by determining suitable parameters for a given specification of a stub filter. It is an illustrative two-state problem, where the parameter-dependent solution either satisfies or fails the specification. The main part of the applications deals with a classical EMC example, namely calculation of the shielding effectiveness of rectangular metallic enclosures. Shielding effectiveness is defined as the attenuation of electromagnetic energy due to the enclosure. Three enclosures are considered, each under plane-wave illumination of various incident angles and frequencies of the electromagnetic field. We find that the external field easily penetrates into the modelled enclosures and, due to resonance phenomena, enclosures sometimes even amplify the field. In addition, we introduce amplitude histograms to study field statistics inside the enclosure. In these studies specifications, the shielding effectiveness and distances between histograms have been used as moms. Finally, the idea of partitioning and the parameter space description is connected to a general context of partial differential equations describing wave-like phenomena.

Chapter 2

Partitioning and implementation

In this Thesis, the solutions and input parameters of simulations are grouped into a small number of classes according to values of a real-valued grouping function, a measure of merit (mom). The partition of a set is defined as a collection of distinct nonempty subsets, which covers the original set [6]. For an interval $[a, b]$, a partition is a finite set of points $\{x_0, x_1, ..., x_n\}$ such that $a = x_0 < x_1 < ... < x_n = b$. In our classification scheme the input parameters mapped onto a given interval constitute a class in the partitioning of the parameter space. In addition to the physical parameters, we need to consider parameters related to the numerical implementation of the model. Simulation results, and hence the partitioning, depend on the implementation. Below, we discuss mainly recursive simulations such that the implementation parameter can be the number of volume elements of a finite element model (FEM). Successive partitionings can be compared by using intersections of the classes of different iterations. We also present a tool for visualisation of the evolution of partitionings.

2.1 Partitioning the parameter space

Let us introduce the parameter space M, where the coordinates correspond to the parameters of a given model. The original model F is introduced as a mapping $F : M \to V$, where V is the solution space. Later on, we shall redefine it as $F : M \times I \to V$, where I is the implementation space used for identifying

the implementation parameters. In most applications, the parameter space is the space R^n and the implementation space is R^k, where n is the number of parameters and k is the number of implementation parameters. We choose a set of parameter vectors, the input, from a compact subset $B \subset M$ and denote it by S.

The partitioning is constructed by ordering the simulations according to a mom function $d : V \to R$. The classes are induced by partitioning the image of the mom, which we denote by $J = [\min((d \circ F)(S)), \max((d \circ F)(S))]$ and partition into m subintervals. We characterise the features of the simulation model by defining an equivalence relation between two input vectors x_1 and x_2 as

$$x_1 \sim x_2 \Leftrightarrow (d \circ F)(x_1) \cong (d \circ F)(x_2), \tag{2.1}$$

where $\cong$ means that the images $(d \circ F)(x_1)$ and $(d \circ F)(x_2)$ belong to the same subinterval of J. The inverse images of the subintervals give the classes of the input vectors. The partitioning obtained this way can be used to construct a covering of the set B in the physical parameter space [III]. If one or a few simulations fail, we group them into the class of failed simulations, the class $m + 1$. Also, poorly converged simulations can be assigned to that "crash" class. Different realisations of this procedure are discussed in Papers [I–VI]. For partitioning of large data sets there exist several advanced methods, e.g. clustering of self-organised maps [7] and pattern analysis techniques [1, 2, 3].

However, with data such as sounds, fingerprints etc., the selection of mom as well as the indexing of the data would be very difficult [8]. To describe the overall results, we introduce a simulation state vector Ψ. When the input is partitioned into the m subsets, it reads

$$\Psi = \sum_{i=1}^{m+1} c_i[r_i], \tag{2.2}$$

where $[r_i]$ stands for the class i, r_i and c_i are the representative and the weight of this class, respectively. The l^1 norm of the state vector defined as $\|\Psi\| = \sum_{i=1}^{m+1} |c_i|$ is used in the analysis of partitionings. If the parameters are uniformly distributed over the set B, the probability that a new simulation will yield the result in the i^{th} class can be estimated by using the class weight c_i.

This kind of grouping induces classes with strict limits. For a more flexible interpretation techniques such as fuzzy association, nearest- or k$^{\text{th}}$-nearest-neighbour association and centred association can be used [2, 4].

2.2 Correlation between different moms

After the partitioning task is completed, it is natural to ask whether two partitionings are similar, in other words, do the corresponding moms correlate. In order to compare the moms, both partitionings should have the same number of classes. Otherwise, a necessary number of empty classes can be created to facilitate one-to-one correspondence [9]. For instance, in the equal length partitioning of the intervals $[\min(d_s \circ F), \max(d_s \circ F)]$, the classes can be indexed by increasing values of moms.

We introduce two correlation measures between partitionings as a set comparison between the classes. First, we define the classwise correlator as

$$\langle d_1, d_2 \rangle_{\mathrm{cl}} = \frac{1}{m} \sum_{i=1}^{m+1} \frac{|\{r_i^1\} \cap \{r_i^2\}|}{|\{r_i^1\} \cup \{r_i^2\}|}, \tag{2.3}$$

where $\{r_i^1\}$ refers to the i^{th} class obtained by the first mom and $\{r_i^2\}$ refers to the i^{th} class obtained by the second mom and $|\cdot|$ denotes the measure of a set in the parameter space, here usually the number of input points in the set [III]. For empty sets, we must use $|\emptyset|/|\emptyset| = 1$. The pointwise correlator is defined as

$$\langle d_s, d_{s'} \rangle_{\mathrm{p}} = \frac{1}{N} \sum_{i=1}^{m+1} |\{r_i^s\} \cap \{r_i^{s'}\}|, \tag{2.4}$$

where N is the total number of input points. While the classwise correlator emphasises the similarity of each class, the pointwise correlator directly evaluates the number of identical classifications. These correlators can be used to identify quantities that behave in a similar manner.

2.3 Visualisation

We illustrate the stabilisation of the partitioning by constructing a visualisation graph, which depicts the connections between the classes obtained at different iterations [I]. The visualisation graph describes the dynamics of partitionings as a function of implementation. In literature, there exist other visualisation structures like vector bundles and α-shapes [10, 11, 12, 13].

Let the implementation space be $I = R^k$. For a recursive process the successive implementations can be replaced by real numbers $\{k_0, k_1, ..., k_h\}$, where the set of implementation indices $\{0, 1, ..., h\}$ can be used for identifying different iterations.

Next, we repeat the construction presented in paper I. Let us have a mom function $d : V \to R$, a partitioning to m classes, model F and input S. Let $p \in S$ be arbitrary and let the model be solved recursively, using p as an input for $h + 1$ times. The corresponding input can be given as a sequence on $p \times I$ and it can be denoted as $p_0, p_1, ..., p_h = (p, I(k_0)), (p, I(k_1)), ..., (p, I(k_h))$. The results of successive implementations are compared as follows:

- The mappings $d \circ F(p_l)$ and $d \circ F(p_{l+1})$ applied to $\forall p \in S$ determine two partitionings on the parameter space with respect to implementations k_l and k_{l+1}.
- If $d \circ F(p_l)$ belongs to the same class as $d \circ F(p_{l+1})$, we say that implementations I_l and I_{l+1} are equivalent with respect to p. If two implementations are equivalent $\forall p \in S$, they are equivalent with respect to the input S.
- The dynamics of the class structure and the partitioning are studied by arranging the results of the steps above as a series with respect to the implementation index $l = 0, ..., h$.

If the parameter space is two-dimensional, the visualisation of the class structure can be realised in R^3 so that the parameter space is identified with the bottom plane and the vertical axis refers to the implementation index. In higher dimensions, we can use a two-dimensional projection of the parameter space and visualise the structure on it. Similar hierarchial structure for data presentation in the case of data mining is presented in [14].

The visualisation graph is defined as a distinct collection of the m class representatives, i.e., excluding the crash class. The vertices are labelled by $p^{(k,i)}$, where k is the implementation index and i is the class index. Vertices corresponding to the same value of the implementation index are distinct. If there is at least one common point in the classes represented by $p^{(k,i)}$, and $p^{(k+1,j)}$, these vertices will be connected by a line. The visualisation graph is given by the vertices and their connections on $R^2 \times \{0, 1, ..., h\}$.

2.4 Partitioning stability

The stability of the partitioning with respect to the implementation means that for most points in the input S the classification does not change for successive iterations. If stabilisation is not achieved in the visualised picture, the accuracy of the partitioning can be estimated using a set of similarity measures [15]. Now we include the crash class to the discussion. Let the set of vertices at the k^{th}

implementation index be denoted by $W(k)$ and consider a class of mappings $\lambda^{(k,k')} : W(k) \times W(k') \to GL(m+1)$, where $GL(m+1)$ is the general group of $(m+1) \times (m+1)$ matrices.[1] We require that matrices satisfy the following rules:

- $\lambda^{k,k} = 1_{m+1}$ is an $(m+1) \times (m+1)$-identity matrix.
- $\lambda^{k,k+1} = 1_{m \times m}$ for a sufficiently large $k > k_0$ so that the simulation becomes asymptotically implementation free.
- The element $\lambda^{k,k'}(i, m+1)$ corresponds to the simulations from the i^{th} class on the implementation level k failed before or on the k'^{th} level.

The probability of finding an arbitrary parameter point of $\{p^{(k,i)}\}$ from $\{p^{(k',j)}\}$, and its matrix elements are given by

$$\lambda_1^{k,k'}(ij) \equiv P\left(p^{(k,i)} \to p^{(k',j)}\right) = \frac{|\{p^{(k,i)}\} \cap \{p^{(k',j)}\}|}{|\{p^{(k,i)}\}|}. \tag{2.5}$$

No elements of the set $\{p^{(k,i)}\}$ disappear, so that $\sum_{j=1}^{m+1} \lambda_1^{(k,k')}(ij) = 1$. If the class of failed simulations consists only of crashed simulations, which cannot be recursively continued, then $\lambda^{k,k'}(m+1, i) = 0 \ \forall \ i > 1, \ \text{and} \ k > k'$. The matrix defined by Eq. (2.5) is not symmetric with respect to exchange of implementation indices. Two kinds of symmetric mappings have been introduced [I, II]:

$$\lambda_2^{k,k'}(ij) = \frac{|\{p^{(k,i)}\} \cup \{p^{(k',j)}\}| - |\{p^{(k,i)}\} \cap \{p^{(k',j)}\}|}{|\{p^{(k,i)}\}| \cup \{p^{(k',j)}\}|} \tag{2.6}$$

$$\begin{aligned} 2\lambda_3^{k,k'}(ij) &= \frac{|\{p^{(k,i)}\} \cup \{p^{(k',j)}\}| - |\{p^{(k,i)}\} \cap \{p^{(k',j)}\}|}{|\{p^{(k,i)}\}| \cup \{p^{(k',j)}\}|} \\ &+ \frac{|\{p^{(k',i)}\} \cup \{p^{(k,j)}\}| - |\{p^{(k',i)}\} \cap \{p^{(k,j)}\}|}{|\{p^{(k',i)}\}| \cup \{p^{(k,j)}\}|} \end{aligned} \tag{2.7}$$

The mappings $1 - \lambda_2$ and $1 - \lambda_3$ satisfy the properties listed above. These sets of matrix elements are applicable when estimating the stability of partitioning.

Mutual comparison of two partitionings can be achieved by comparing the corresponding state vectors in Eq. (2.2). Denoting the state vector corresponding the implementation index k by Ψ^k, the l^1 norm of the difference vector, $||\Psi^k - \Psi^{k'}||$, introduces a metric between two groupings. Even if the stability (convergence) of the grouping with respect to the norm is obtained, i.e,

[1] In papers I and III the set of vertices $W(k)$ is denoted by $ISC(k)$.

$\|\Psi^k - \Psi^{k'}\| = 0$ for sufficiently large indices k and k', it still does not guarantee the stability of the partitioning. Let us improve the "convergence" criteria and introduce another state vector:

$$\begin{aligned}\chi^{k,k'} \quad := \quad & (\lambda_1^{k,k'}(1,1) - 1, \lambda_1^{k,k'}(1,2), \ldots, \lambda_1^{k,k'}(1,m+1), \lambda_1^{k,k'}(2,1), \\ & \lambda_1^{k,k'}(2,2) - 1, \ldots, \lambda_1^{k,k'}(m+1,m+1) - 1). \end{aligned} \tag{2.8}$$

When the norm $\|\chi^{k,k'}\|$ converges towards zero, also visual convergence criteria are met, i.e., the visualisation graph has no connecting lines (branches) between different vertices. Thus, the state vector $\chi^{k,k'}$ is a better indicator of the convergence of the simulation.

Chapter 3

Two-class partitioning

We consider next a specific example of binary classification, where the parameters are grouped into two classes. As a case study, we choose a specification determination of a stub filter, see Fig. 3.1 below and Papers [II, III]. This example demonstrates the introduced methodology. A specification is a property that a system of interest has to fulfill. In its simplest form, a specification is given by a real-valued function, and the measure of merit can be taken to be the specification. Then, for a well-defined parameter space our method can be applied directly. Acceptable parameters are those, which satisfy the given specification. The input parameters are grouped into the classes $[r_1]$ and $[r_0]$ according to whether the specification is fulfilled or failed, respectively. The visualisation graph reduces to a two-vertex model and looks like stairs, so we shall call it the implementation stairs.

3.1 A stub filter

Let us consider a specification determination of a stub filter. Stub filters are widely used in electronic devices to create required response between the input and output voltages. The stub filter produces an attenuation of incoming voltage in a certain frequency interval, depending on the length of the stub and the frequency. These two are the natural parameters of the problem. The problem can be described by a scattering matrix S

$$\begin{pmatrix} S_{11} & S_{12} \\ S_{21} & S_{22} \end{pmatrix} \begin{pmatrix} V_1^+ \\ V_2^+ \end{pmatrix} = \begin{pmatrix} V_1^- \\ V_2^- \end{pmatrix}, \tag{3.1}$$

where the ingoing voltage is denoted by V^+ and outcoming by V^-. The relative attenuation is given by the matrix element S_{21}, which we select to be the measure of merit. We select randomly 699 parameter vectors as an input. The parameter values are restricted to the intervals [1 GHz, 3 GHz] for frequency and [12.0 mm, 40.0 mm] for stub length, respectively. The structure of the filter is shown in Fig. 3.1.

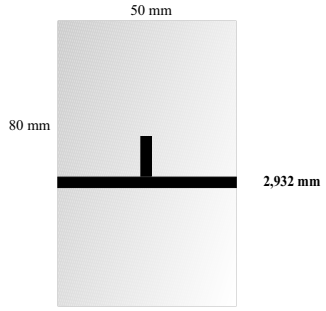

Figure 3.1: A stub filter constructed using microstrip lines on a dielectric. In the figure the dielectric is grey, the microstrips are black, the input voltage is brought at the left (or right) end of the device and the output voltage is measured at the right (or left) end. In numerical simulations, the filter was surrounded by a computational cube.

The following properties define the boundary conditions of the problem: The filter has 50 Ω microstrip lines, the conductors on the microstrip are assumed to be of zero thickness and infinite conductivity. The length of the microstrip is 50.0 mm and the width 2.932 mm in order to be compatible with 50 Ω ports. The microstrip lines are placed on a dielectric substrate ($\epsilon_R = 4.4$) of size $50.0 \times 80.0 \times 1.6$ mm^3 ($L \times W \times H$). The system is embedded in a computational cube with dimensions $50.0 \times 80.0 \times 80.0$ mm^3. The cube is filled with air and two of its opposite facets define the 50 Ω ports, while other facets are assumed to be perfect conductors.

The model is solved by a commercial high frequency simulation software Ansoft HFSS 8.0 which was controlled by MATLAB [16]. We identify the number of tetrahedra of the simulation mesh as the one-dimensional implementation parameter and calculate 15 recursive simulation steps. The number of tetrahedra varied in the first implementation from few hundreds up to thousand and in the 15^{th} implementation from few thousand up to fifteen thousand depending on the input parameters.

3.2 Results for the stub filter

Two classes are determined by the chosen mom S_{21} and they are indexed by one for accepted $[r_1]$ and by zero for rejected $[r_0]$ parameters. Two threshold values of mom, 20 and 30 dB, are considered. Four partitionings corresponding to different implementations are depicted in Fig. 3.2.

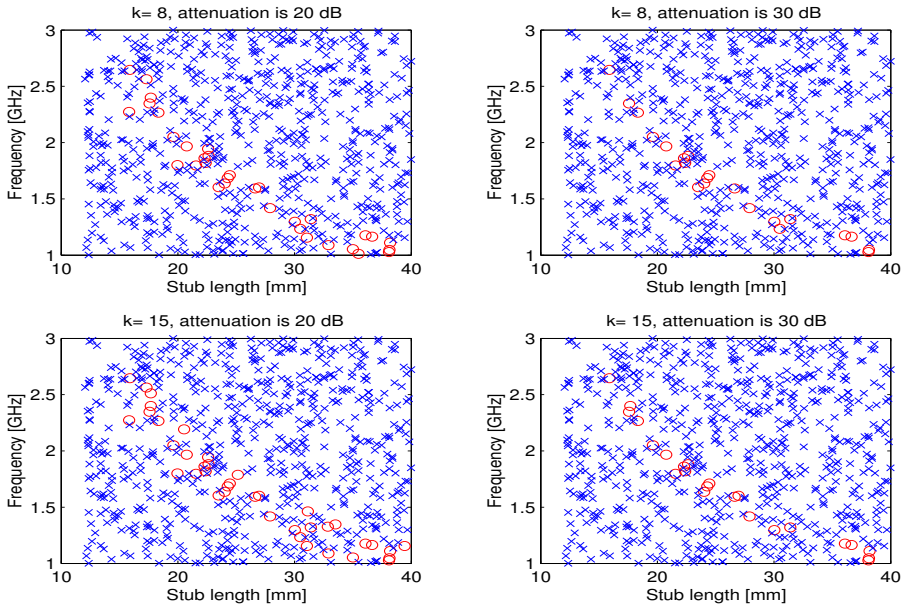

Figure 3.2: Four partitionings with attenuation threshold values 20 dB and 30 dB. The upper plots are partitionings obtained at the eighth ($k = 8$) iteration, and the lower ones correspond to the 15^{th} ($k = 15$) iteration. The accepted parameters corresponding to the class $[r_1]$ are denoted by red circles and those corresponding to the class $[r_0]$ by blue stars.

The stability of the partitioning is examined using λ_1 for 20 dB attenuation, and $1 - \lambda_3$ for 30 dB attenuation. For example, the diagonal elements of the matrix $\lambda_1^{3,4}$ give the proportion of input parameter vectors preserved in same classes by the fourth iteration, while the off-diagonal elements describe the changes in the partition. The following sequences of matrices show that the stability is rather good in both cases. Explicitly, these matrices read

$$\lambda_1^{3,4} = \begin{pmatrix} 0.8636 & 0.1364 \\ 0.0089 & 0.9911 \end{pmatrix} \qquad \lambda_1^{8,9} = \begin{pmatrix} 1.0000 & 0 \\ 0.0045 & 0.9955 \end{pmatrix}$$

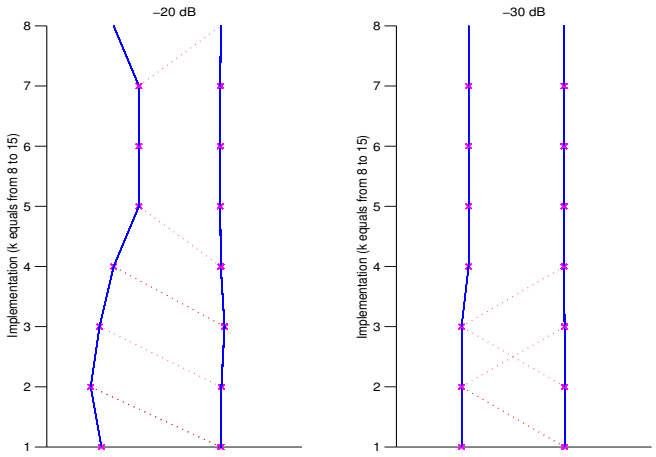

Figure 3.3: Visualisation of the classes and their dynamics in a one-dimensional projection of the parameter space by a two-vertex model. The vertices (red crosses) are the class representatives, which are connected between successive implementations if the corresponding classes share common input vectors. The implementation stairs on the left correspond to attenuation of 20 dB and on the right to 30 dB attenuation. The direction of the projection has been chosen to emphasise the stairlike structure. The vertical axis begins at the 8^{th} implementation and the value 8 corresponds to the 15^{th} iteration.

$$\lambda_1^{9,10} = \begin{pmatrix} 1.0000 & 0 \\ 0.0015 & 0.9985 \end{pmatrix} \qquad \lambda_1^{10,11} = \begin{pmatrix} 1.0000 & 0 \\ 0.0030 & 0.9970 \end{pmatrix}$$

$$\lambda_1^{11,12} = \begin{pmatrix} 1.0000 & 0 \\ 0.0015 & 0.9985 \end{pmatrix} \qquad \lambda_1^{12,13} = \begin{pmatrix} 1.0000 & 0 \\ 0 & 1.0000 \end{pmatrix}$$

$$\lambda_1^{13,14} = \begin{pmatrix} 1.0000 & 0 \\ 0 & 1.0000 \end{pmatrix} \qquad \lambda_1^{14,15} = \begin{pmatrix} 0.9750 & 0.0250 \\ 0 & 1.0000 \end{pmatrix}$$

$$1 - \lambda_3^{3,4} = \begin{pmatrix} 0.4615 & 0.0050 \\ 0.0050 & 0.9899 \end{pmatrix} \qquad 1 - \lambda_3^{8,9} = \begin{pmatrix} 0.9167 & 0.0014 \\ 0.0014 & 0.9970 \end{pmatrix}$$

$$1 - \lambda_3^{9,10} = \begin{pmatrix} 0.9200 & 0.0014 \\ 0.0014 & 0.9970 \end{pmatrix} \qquad 1 - \lambda_3^{10,11} = \begin{pmatrix} 0.9583 & 0.0007 \\ 0.0007 & 0.9985 \end{pmatrix}$$

$$1 - \lambda_3^{11,12} = \begin{pmatrix} 1.0000 & 0 \\ 0 & 1.0000 \end{pmatrix}$$

The symmetric matrices $(1 - \lambda_3)$ after the 12^{th} iteration are identity matrices,

so the partitioning appears to have stabilised, see also Fig. 3.3. The geometrical centroids of the classes are chosen to be the representatives r_1 and r_0. Because the classes are disconnected, these representatives do not provide a complete picture of the positions of the classes in the parameter space. The parameter space has been projected onto a single dimension in order to clarify the visualisation.

This approach to specification determination problems can be used to restrict the number of configurations in further optimisation. If more than one specification is needed, the partitioning can be done with respect to all independent specifications, possibly simultaneously. The convergence matrices give valuable information about the number of required iterations.

Chapter 4

Shielding effectiveness of rectangular enclosures

We are surrounded by electromagnetic radiation consisting of a broad range of frequencies. To proceed into electromagnetic compatibility (EMC) and shielding effectiveness, let us consider radiation at frequencies between few MHz and several GHz. For instance mobile phones function within this frequency interval, and they also provide a typical EMC example by interfering other equipment during phone calls. What happens there? Actually, there is no simple direct answer to this question, but the external radiation couples with the equipment, thus disturbing its function. Therefore, sensitive electronics should be enclosed inside shielded cavities. When the electronics is closed inside a cavity, the interfering field penetrates through holes or is conducted by wires into the cavity. This leads us to a classical EMC topic, namely the shielding effectiveness of a rectangular enclosure with apertures.

An ideal solution to protect electronics would be a closed, perfectly conducting enclosure. However, in practical applications all enclosures contain apertures for ventilation, wiring, accessories, connectors and cooling apparati and no real enclosure has perfectly conducting walls. The determination of the level of penetration in case of a real enclosure is so complex a task that considerable simplifications and approximations are needed. An obvious quantity to study is the electromagnetic power entering an empty enclosure. The ratio of the electromagnetic energy level inside and outside the enclosure is called shielding effectiveness (SE), usually given in decibels. For enclosures, the shielding effectiveness can be determined in terms of electric or magnetic fields. In order

to describe the fields entering the enclosure, one usually adopts the concepts of front-door and backdoor coupling. The front-door coupling stands for coupling via the intentional apertures, antennas etc., while the backdoor coupling refers to unintentional coupling, e.g. through seams and bolts.

Many different techniques to reduce the amount of electromagnetic energy inside the cavity exist. These include structural-like, such as shielded enclosures, and covering-like, e.g. conductive coatings, shielding paints. Various solutions are discussed in Ref. [17], and new techniques appear constantly. One new technique to make shielding covers is introduced in Ref. [18], where the authors consider transparent metal foils of thickness in the range of nanometers.

In general, the level of reduction of the electromagnetic energy can be determined using measurements or several modelling techniques. In order to make measurements and modelled results comparable, standards of shielding effectiveness determination have been introduced [19, 20, 21]. When a high shielding effectiveness is needed, the designing procedure itself consists of several rules, which are discussed for instance in Ref. [22].

4.1 Review of enclosure studies

Shielding effectiveness of the enclosure can be estimated analytically, numerically or experimentally. Analytical methods include e.g. transmission line analogy [23, 24] and circuit theory [25, 26]. A simple a rectangular enclosure with an aperture at one face can be modelled by an equivalent circuit [26], to predict the shielding effectiveness as a function of the frequency and the size of the aperture. The size of the enclosure is often expressed in units of the wavelength of the radiation, commonly known as the electrical size of the enclosure. The apertures can behave like antennas, and their electrical size can be defined analogously to that of antennas [27]. An antenna, which can be contained within a sphere whose diameter is small compared to the wavelength at frequency of operation, is electrically small. When apertures are very small in some directions, their direct implementation in a computer program is not possible and they have to be included for instance as sources. The most convenient way is to replace the aperture by a magnetic and an electric dipole, which are placed inside the enclosure [28]. Such an implementation in shielding effectiveness studies can be found e.g. in Refs. [29, 30]. If the diameter of the aperture is larger than $\lambda/4$, it is usually considered as an electrically large aperture [31]. The enclosure, in turn, is considered to be electrically small as long as its largest dimension is smaller than a few wavelengths at frequency of operation and there are no

overlapping modes inside the enclosure. A threshold value for electrically large enclosures is proposed to be six wave-lengths [32]. At higher frequencies the field behaviour becomes very complex and it should treated statistically. The opposite case, i.e., electrically small enclosures, is studied in Refs. [24, 33]. For a given enclosure, one can define a cut-off frequency as $\nu_0 = c/d$, where c is the speed of light and d is the largest dimension of the enclosure. If the frequency is below the cut-off frequency, shielding effectiveness can be examined using diffraction theory [28, 34].

When experimental work is time consuming and analytical expressions become too complicated, numerical methods provide a practical way to estimate the shielding effectiveness. Among the numerical techniques, the most common are transmission line analogy or method (TLM), FDTD method (finite difference time domain) [35], method of moments [36] and FEM (finite element method) [37]. All these methods can be used and the optimal choice depends on the purpose. For instance, if one needs to collect large amount of spatial information of the field values inside the enclosure, FDTD and FEM will do the task best. They both require the discretisation of the whole computational domain. Usually FDTD runs on time domain and FEM on frequency domain. In the following examples we use FEM, because we want to consider electromagnetic field amplitudes at a given frequency. Naturally, methods can be combined to form hybrid methods. For an example of a hybrid method based on FDTD and FEM on time domain, see Ref. [38]. A recent example of a hybrid method in time domain can be found in Ref. [39], where a combination of method of moments in time domain and FDTD is presented and applied to estimation of shielding effectiveness of complex enclosures. Further examples of different methods are given in Refs. [23, 40, 41, 42] and a comparison of the methods in Refs. [43, 44]. Shielding effectiveness of enclosures has been studied as a function of the frequency and the number of apertures in Refs. [30, 45, 46, 47].

When dimensions of the enclosure are close to a multiple of the wavelengths, a resonance may occur. In other words, the enclosure starts to resonate like a musical instrument and the field inside increases. Thus, at resonance frequencies, shielding effectiveness decreases and may even become negative. Therefore, it is important to recognise the resonance frequencies of the enclosure and study the shielding effectiveness at these "worst" frequencies. A simple estimate for resonance frequencies of an empty cavity obtained from [48]

$$\nu_{\text{res}} = \frac{c}{2}\sqrt{\sum_{i=1}^{3}(n_i/l_i)^2}, \tag{4.1}$$

where l_i is the ith dimension of the enclosure, c is the speed of light, and the numbers n_i are non-negative integers with the restriction that no more than one can be simultaneously zero. A standing wave inside the enclosure is called a mode. When different modes cannot be separated from each other, the field is said to be overmoded. Numerical shielding effectiveness studies concentrating on resonance modes can be found in Refs. [23, 49]. Expectedly, simulations show the reduction of shielding effectiveness at high frequencies. Statistical studies of overmoded enclosures are reported in Refs. [31, 50, 51].

In order to consider more realistic models of enclosures, the internal structure has to be taken into account and numerical results should be verified by measurements. A good comparison of experimental and numerical studies can be found in Ref. [52]. A well-shielded enclosure with complex internal structure was examined in Ref. [29], where a piece of absorbent was placed inside the enclosure together with small internal receiving antennas. In Refs. [39, 53, 54], a printed circuit board and conducting planes were added inside the enclosure. The effect of large apertures of arbitrary size has been studied in Ref. [55], where different loss mechanisms inside the enclosure were considered. Naturally, the transmission of the external field into the enclosure depends on the apertures, their size, direction with respect to field polarisation and incoming radiation and of course the number of the apertures.

The shielding effectiveness of an enclosure can defined as

$$\mathrm{SE} = -20\log(E/E_0) \tag{4.2}$$

$$\mathrm{SE} = -20\log(H/H_0) \tag{4.3}$$

$$\mathrm{SE} = -10\log(P/P_0), \tag{4.4}$$

in terms of electric and magnetic field and electromagnetic power, respectively. Here E is the electric field at a given point inside the enclosure, and E_0 refers to the corresponding electric field in the absence of the enclosure, H is the magnetic field inside the enclosure and H_0 is the corresponding reference value. Furthermore, P is the power inside the enclosure and P_0 is the reference value. In all cases, it measures the attenuation of power associated to the presence of the enclosure. Usually SE is considered at one particular point, e.g. at the centre. Alternative expressions for shielding effectiveness, e.g. using L^p-norms of the fields, have been proposed in Refs. [56, 57].

4.2 Statistics of the electric field

Let us discuss briefly the electromagnetic field inside electrically large enclosures and reverberation chambers. Reverberation chambers are used to create direction-independent electromagnetic field for electronics testing. As discussed above, the field inside electrically large enclosures becomes overmoded, so statistical description is needed [58, 59]. The statistical treatment of electromagnetic modes leads to a theory called statistical electromagnetics. The field statistics inside electrically large enclosures were first discussed in early 90's in Refs. [51, 60].

Inside an electrically large enclosure, almost all frequencies create resonances, thus amplifying the field. A quantity that relates the properties of the enclosure to the amplification is the quality factor Q of the enclosure. It is defined as [31, 55]

$$Q = \omega \frac{\text{time average of the restored energy in system}}{\text{energy loss rate in system}}, \tag{4.5}$$

where $\omega = 2\pi f$ and f is the frequency of the electromagnetic field. Alternatively, the Q-factor can be defined as the half-width of the peak around the resonance frequency. Assume a single wave excitation and the system in a steady state, i.e., the power transmitted through apertures equals to the power dissipated due to absorptions, leaks through apertures etc. The Q-factor can be related to shielding effectiveness study for uniform energy density inside the enclosure if Q-factor and transmission cross section are known [55, 61].

Another application of the statistical analysis is to describe electromagnetic field inside reverberation chambers, which are used e.g. in electromagnetic immunity testing [62]. In order to test different initial conditions without rotating the test object, isotropic, randomly polarized, and statistically uniform electromagnetic field is needed. The mode stirring is considered in Ref. [63], the plane wave representation of the EM field inside the chamber in Refs. [64, 65], and spatial correlations of fields and energy density in Refs. [66, 67]. Statistics of the fields and the Q-factors are discussed in Refs. [68, 69, 70]. Statistical and histogram approach as applied to shielding effectiveness and reverberation chambers have been discussed in Refs. [71, 72, 73]. Experimental and theoretical results have been compared in Refs. [74, 75].

Field statistics inside electrically large enclosures have been extensively studied. The statistics can be derived for the electric field components or for the electric field amplitudes. In general, the field can be expressed as a linear combination of the eigenmodes corresponding to two independent polarisation states

and the expectation values equal to volume averages as shown in Ref. [60]. This holds, when the locations, where the field values are determined, are uniformly distributed inside the enclosure. In Ref. [60], the probability distribution function of the time averaged component of the electric field is shown to be normally distributed. Because the field components consist of two independent polarisation states, the magnitudes of electric field components follow the Rayleigh distribution. The total field follows χ statistics with six degrees of freedom and the probability distribution for the electric power (E^2) is the χ^2 distribution. Further analysis is carried out in Refs. [31, 50, 51] and references therein. However, the evaluation of the electric field statistics inside a rectangular enclosure with apertures is still under development.

When the enclosure is not electrically large, the field cannot be predicted from simple expressions or by any of the methods discussed so far. In chapter 5 we shall propose an alternative histogram approach in order to extract some qualitative information on the field statistics.

4.3 Practical examples

We move on to some examples of shielding effectiveness of rectangular enclosures. We determine the shielding effectiveness using simulated electromagnetic field values inside two different geometries. We call these geometries "PC" and "345". The "PC" resembles an enclosure of a common PC and the other one is called to "345" according to its dimensions. The size of the PC enclosure shown in Fig. 4.1 was 450 mm $\times$ 450 mm $\times$ 200 mm, and the size of the power supply inside it was 160 mm $\times$ 150 mm $\times$ 150 mm. In Paper [IV] we also considered the PC geometry without the power supply. The apertures' dimensions were 15 mm $\times$ 120 mm for the upper one, and 15 mm $\times$ 90 mm for lower ones. The size of the 345-enclosure shown in Fig. 4.2 was 300 mm $\times$ 400 mm $\times$ 500 mm and the size of the aperture was 120 mm $\times$ 15 mm.

In these studies the shielding effectiveness is used as a measure of merit. We also consider field distributions inside the enclosures. The dimensions of the enclosures and the sizes of the apertures are sufficiently large, so the shielding effectiveness is not expected to be very good in the considered frequency interval. In simulations we identify the implementation with the number of tetrahedra in the simulation mesh. The shielding effectiveness is calculated either from the mean value of the electric field or the peak value of the electric field.

The solutions are obtained by solving the Maxwell equations without external currents, when the enclosures are under external illumination, which is

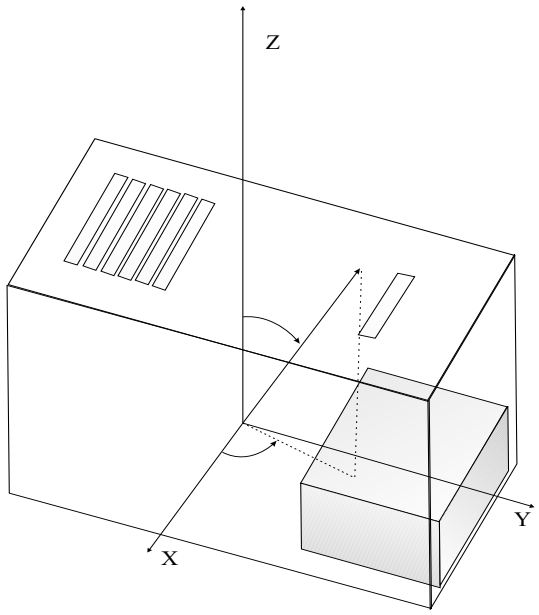

Figure 4.1: The PC geometry. The grey box represents the power supply.

assumed to be a time-harmonic plane wave. The boundaries of the enclosures are modelled as perfect conductors, but also steel boundaries have been considered [IV]. The models are solved using commercial high frequency software Ansoft HFSS 7.0 (the example in section 4.3.1) and 8.0 (elsewhere).

4.3.1 A study at 1 GHz frequency

The first set of input parameters for PC geometry consisted of 200 vectors chosen from the parameter space of incident plane wave. The enclosure was positioned such that the aperture side was perpendicular to the z-axis. The plane waves were characterised by the wave vector $\mathbf{k}$, which is determined by the frequency $\nu = 1$ GHz and the coordinates (θ, ϕ), which define the initial conditions. The amplitudes $\mathbf{E}_0$, $\mathbf{B}_0$ and the wave vector $\mathbf{k}$ define a right-handed coordinate system fixed by setting $\mathbf{E}_0 \uparrow\uparrow \hat{x}$ at $(\theta, \phi) = (0, 0)$. The aim was to find the angular dependency at a given frequency. The number of tetrahedra varied here between 4500 and 35000 and nine consequtive implementations were executed. In this subsubsection, we use a modified expression for the shielding

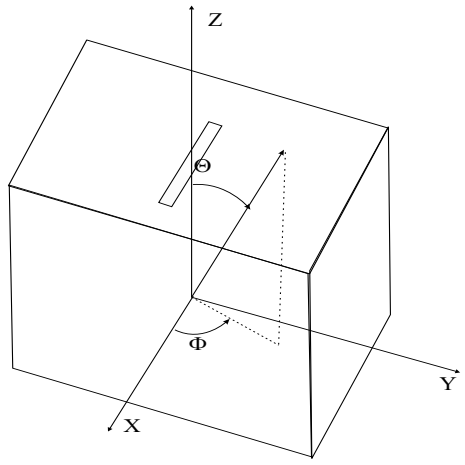

Figure 4.2: The 345-enclosure with a single aperture.

effectiveness, namely [I]

$$\mathrm{se} = -10 \log \left(\frac{2}{\pi V} \int_V |E/E_0| dV \right), \tag{4.6}$$

where V is the inner volume of the enclosure, E is the electric field amplitude and E_0 is the electric field reference level set to 1 V/m.

The analysis in Paper [I] shows that the coordinate θ does not significantly affect shielding effectiveness. Let us now set the limiting values of mom in Eq. (4.6) to 0 and 10 and examine the stability of the obtained partitionings. The partitionings in Fig. 4.3 are obtained for implementations $k = 6, 7, 8, 9$.

We illustrate the stability of the partitionings by showing the corresponding λ matrices for the two final implementations:

$$\lambda_1^{8,9} = \begin{pmatrix} 1 & 0 & 0 \\ 0.0219 & 0.9635 & 0.0073 \\ 0 & 0 & 1 \end{pmatrix}$$

$$1 - \lambda_2^{8,9} = \begin{pmatrix} 0.9375 & 0 & 0 \\ 0.0165 & 0.9635 & 0.0065 \\ 0 & 0 & 0.9412 \end{pmatrix}$$

$$1 - \lambda_3^{8,9} = \begin{pmatrix} 0.9375 & 0.0082 & 0 \\ 0.0082 & 0.9635 & 0.0033 \\ 0 & 0.0033 & 0.9412 \end{pmatrix}.$$

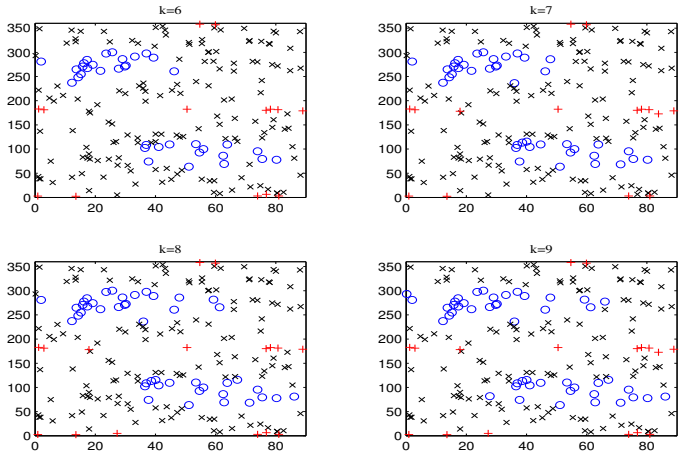

Figure 4.3: Examples of partitionings for the PC geometry. Blue circles correspond to the input parameters, which produce negative mom values, the black x's correspond to the intermediate cases with se $\in [0, 10]$ and red crosses to good se > 10.

We look at the stabilisation of the partitioning by constructing the corresponding visualisation graph shown in Fig. 4.4. Finally, the corresponding simulation vectors were calculated to yield

$$\begin{aligned} \psi^6 &= (\ 0.1800 \quad 0.7450 \quad 0.0700\ ) \\ \psi^7 &= (\ 0.2050 \quad 0.7150 \quad 0.0750\ ) \\ \psi^8 &= (\ 0.2250 \quad 0.6850 \quad 0.0800\ ) \\ \psi^9 &= (\ 0.2400 \quad 0.6600 \quad 0.0850\ )\ . \end{aligned}$$

We observe that the partitioning is almost stable after 9 iterations. This can be seen in the matrix elements as well as the state vector coefficients. Also, no more than 3 percent of the input vectors have changed their classes between 8^{th} and 9^{th} iteration, which can be seen from the expression $\lambda_1^{8,9}$. The symmetry of the geometry with respect to $\phi = 180°$ is reflected in the results. The most harmful direction is $\phi = 90°$ and $\phi = 270°$, where the polarisation of the external field is perpendicular to the apertures.

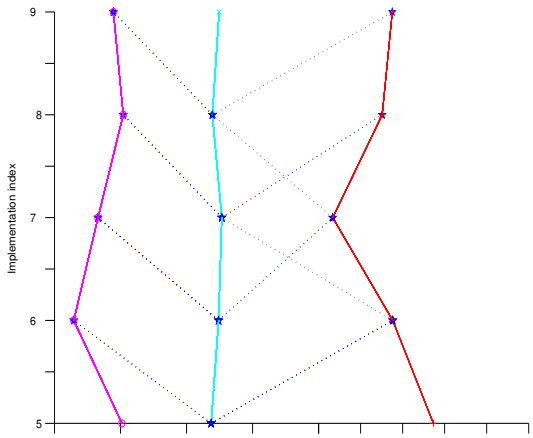

Figure 4.4: The implementation visualisation graph from the 5^{th} to 9^{th} iteration.

4.3.2 Partitions and correlations

Consider next another input set of parameters of 500 parameter vectors for the PC geometry, which are selected from the interval $[0.5, 1.5] \times [0, 180]$ of the parameter space. Here the frequency ν is given in GHz and the spherical angle ϕ in degrees. Encouraged by the first example, the angle θ is set to zero. This means that the radiation propagates in the direction normal to the front side (with apertures) of the enclosure and ϕ determines the polarisation of the electric field. Again, we choose that $E_0 \uparrow\uparrow \hat{x}$, when $\phi = 0$. This simulation is done with twelve recursive iterations and the number of tetrahedra is the implementation variable. At the 12^{th} iteration, number of tetrahedra varied between 9600 and 52800. The electric field values are computed and collected inside the enclosure. Altogether 40500 field values are extracted at sites of a regular lattice. The shielding effectiveness is determined using the mean and peak values of the electric field. The moms are calculated according to $\text{SE} = -20\log(E/E_0)$, where E is the mean/peak value and E_0 is the reference level, again 1 V/m.

The criteria for poor convergence were determined from the ideal relative difference of fields by Ansoft HFSS 8.0. Correlations between obtained partitionings are calculated using Eqs. (2.3) and (2.4) with the classes ordered according to the shielding effectiveness. The class ordering in comparison between different moms is discussed in Ref. [9], where the purpose was to find the maximal correspondence between the groupings given by the histogram approach and the shielding effectiveness. Some values of the correlators can be found in

Paper [III]. For the present example the simulation states at 12^{th} iteration read

$$\psi_{\text{mean}} = (\ 0.0460 \quad 0.3840 \quad 0.2040 \quad 0.2020 \quad 0.1560 \quad 0.0080\ )$$
$$\psi_{\text{peak}} = (\ 0.0160 \quad 0.1200 \quad 0.4080 \quad 0.3320 \quad 0.1160 \quad 0.0080\ ).$$

We observe that the mean value classifies the input points more evenly in the shielding effectiveness interval that the peak value. The norms of the convergence state vectors corresponding to peak value shielding effectiveness are presented in Table 4.1. The norms on the final iteration were $\chi_{\text{mean}}^{11,12} = 1.5641$ and $\chi_{\text{peak}}^{11,12} = 2.3019$, and the mean value mom appears to behave more smoothly in all cases [III].

Table 4.1: The simulation state coefficients c_i and corresponding convergence values for the iterations 8-12. The values are related to calculations of shielding effectiveness using the peak value of the electric field inside the enclosure.

Iteration k	8	9	10	11	12
c_1	0.0480	0.0460	0.0400	0.0180	0.0160
c_2	0.2700	0.2720	0.2580	0.1480	0.1200
c_3	0.3160	0.3180	0.3100	0.3940	0.4080
c_4	0.2460	0.2460	0.2760	0.3200	0.3320
c_5	0.0920	0.1000	0.1040	0.1100	0.1160
c_6	0.0280	0.0180	0.0120	0.0100	0.0080
$d(k-1,k)$	-	0.0240	0.0680	0.2680	0.0640
$\|\|\chi^{k-1,k}\|\|_1$	-	1.6424	2.4868	3.6725	2.3019
$\|\|\chi^{8,k}\|\|_1$	0	1.6424	3.0209	4.9089	5.6648
$\|\|\chi_{\bar{m}}^{k-1,k}\|\|_1$	-	0.5944	1.1317	2.1161	1.0918

Chapter 5

Histograms of electric field amplitudes

Finally, we consider histograms of electric field amplitudes inside the enclosures. The goal is to compare different histograms and their modifications with shielding effectiveness and search for a correspondence between histograms and shielding effectiveness in terms of partitioning. The field values are obtained from simulations and the field amplitudes are collected inside the enclosures at the lattice nodes of a cubic lattice with lattice constant of 1 cm. In terms of earlier definitions, the considered enclosures were not electrically large at the studied frequencies. Therefore, the results cannot be directly compared with the theory, and the underlying distribution is not necessarily the chi-square distribution [60, 51]. It should be noted that histograms in the context of reverberation chambers have been studied in Refs. [71, 72, 73]. We do the comparison and grouping of the parameters by using a grouping algorithm and introduce four different distance measures between the histograms to be used as moms [IV, VI]. According to the results in Paper [VI] and Ref. [9], certain modifications of the histograms improve their correlation with the shielding effectiveness. In short, we represent a deterministic solution by a histogram. Note that the spatial information is lost. In Fig. 5.1 we show two (unmodified) histograms of the electric field amplitudes inside the PC enclosure.

There is a visual difference between these two histograms, but it is not obvious how it can be expressed in terms of moms. One possibility could be to use distance measures between histograms and in particularly the square-sum differences [76]. By calculating the distances of histograms from a selected

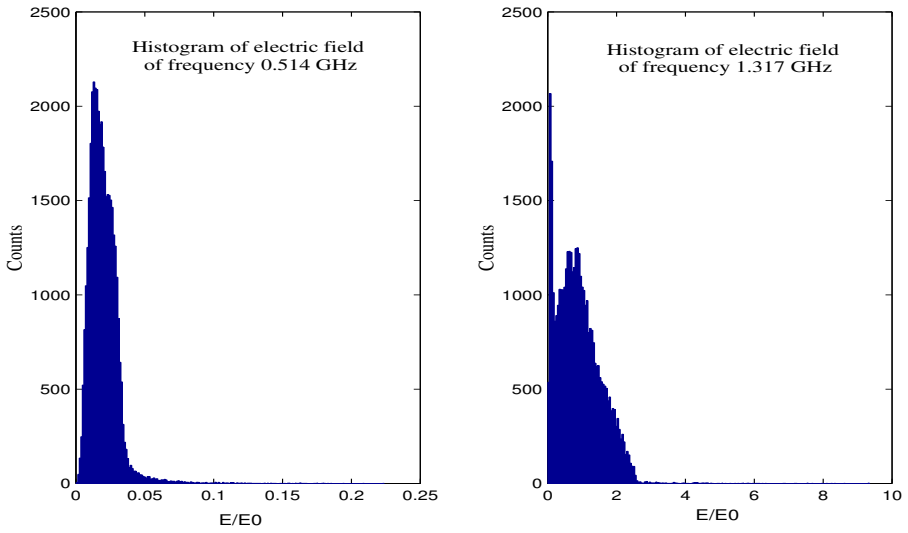

Figure 5.1: Two typical histograms of the electric field inside the enclosure. The left histogram corresponds to frequency $\nu = 0.514$ GHz and $\phi = 171$ and the right histogram to $\nu = 1.317$ GHz and $\phi = 109$. Note the different scales on horizontal axes.

reference histogram, we obtain a real-valued mom [VI, 9]. This way, we end up studying "shapes" of the histograms [78].

5.1 Comparison of the histograms

In order to compare different histograms of the electric field amplitudes inside the enclosures, we introduce the following algorithm [IV, V]:

- The global minimum and maximum values of electric field amplitude provided by a given data set are determined.
- The interval between the global minimum and maximum of the field amplitude is divided into 200 subintervals of equal length to be used as bins in the histograms.
- Each of the distributions is presented by a histogram over the interval and the histograms are filtered by weighted average filter in a following manner. A weighted average was calculated for each bin with weights 1,2,4,2,1 for the bin, its nearest and next-to-nearest neighbours. The filtering is

repeated at least two but no more than ten times. The filtering is stopped once the number of peaks in the distribution histogram doesn't decrease.

- The filtered histograms are scaled to have identical height and width of 20 percent. The width is defined as the length of the interval between the bins, where the value of the bin first increases or last decreases to 20 percent of the maximum bin value of the histogram. The reference histogram is taken to be the histogram with the highest bin.

- The bin-wise square sum differences between the histograms are calculated and the distributions grouped by minimising the squared sum differences in comparison process.

- In the comparison, we start with a reference histogram and calculate the square sums between it and all the other histograms. Then, we determine the maximum square-sum and normalise others by it.

- If the difference between the reference histogram and the histogram under consideration is less than 20 percent of the maximum difference, the histogram is assigned to the group of the reference histogram. Otherwise, the histogram waits till the next iteration. This is continued until all of the histograms have been grouped.

This algorithm can be modified and made more efficient in several ways [VI]. The number of bins is set by hand after some tests. The optimal choice of the number of bins is discussed in Ref. [77]. Finally, we compared groups by using square-sum differences between the reference histogram and other histograms. Explicitly, we set

$$d = \sum_{i=1}^{200} (\bar{h}_i - h_i)^2, \tag{5.1}$$

where $\bar{h}$ is the reference histogram and h is the histogram under comparison. In Paper [VI], alternative rules for the final steps of the algorithm were proposed and tested.

5.2 Applying the histograms

We have used electric field amplitude histograms in several studies [IV, V, VI, 9]. For enclosures we have used both the PC geometry and the 345 geometry as well as some others.

We analysed the effect of the boundary conditions and the relative size on the shape of the histogram. When the frequency becomes close a resonance frequency of the enclosure, the histogram does indeed change remarkably. With the 345 geometry we tested choices of the partitioning and tried to understand physical origins of different shapes of the histograms too. The selection of the partitioning without any a priori purpose or knowledge can be a very difficult task.

As an example, we show here some results for correlations between histograms and shielding effectiveness moms. In Paper [VI] solutions for 290 input frequencies were calculated for the 345 geometry. The partitionings were divided into five groups. In Table 5.1 we show results of an additional test with 300 input frequencies. Some "poorly" converged simulations were considered as a part of one group. The correlations were evaluated between the groupings obtained by shielding effectiveness moms. Qualitatively, the new results are very similar to those in Paper [VI]. Although modifications improve the correlations, the compatibility level between the shielding effectiveness moms is not yet reached. Continuing the studies with further modifications should be useful.

Table 5.1: Pointwise correlations given by Eq. (2.3) and classwise correlations given by Eq. (2.4) between different groupings according to shielding effectiveness and different square-sum distances between the histograms.

Pointwise	*meanse*	*ssdminmax*	*ssdminmean*	*ssdscaled*	*ssdmod*
maxse	0.8200	0.4467	0.3867	0.3700	0.6700
meanse		0.5033	0.3233	0.4033	0.6400
ssdminmax			0.2733	0.6000	0.4333
ssdminmean				0.2433	0.3633
ssdscaled					0.3633
Classwise	*meanse*	*ssdminmax*	*ssdminmean*	*ssdscaled*	*ssdmod*
maxse	0.7502	0.4104	0.3665	0.3605	0.5998
meanse		0.4518	0.3287	0.3821	0.5718
ssdminmax			0.3083	0.5315	0.4008
ssdminmean				0.2849	0.3521
ssdscaled					0.3554

Chapter 6

Partitioning and partial differential equations

We now close the discussion of electromagnetic waves and the numerical EMC problem and next consider mathematical models of wave motion at a more general level. First, we shall discuss the idea of partitioning for linear second order partial differential equations (PDE), after which we proceed to more complicated models and even models with stochastic ingredient.

6.1 Linear second order partial differential equation

As an example, consider the PDE

$$a\frac{\partial^2 h}{\partial y^2} + b\frac{\partial^2 h}{\partial x^2} + c\frac{\partial^2 h}{\partial xy} = 0. \tag{6.1}$$

Our parameter space consists now of the three parameters a, b and c. For this equation, three different kinds of physically motivated sets of solutions can be found. A well-known partitioning can be achieved by studying the derivatives as independent algebraic quantities [79, 80], i.e., by writing

$$a\dot{y}^2 + b\dot{x}^2 + 2c\dot{x}\dot{y} = 0. \tag{6.2}$$

and then considering the discriminant D of the equation, $D = \sqrt{b^2 - ac}$. The discriminant can be negative, positive or zero and it divides the space into three sections as follows. In the xy-plane, we have three different sets of equations: In

the case $b^2 > ac$, the characteristics are hyberbolic, for $b^2 < ac$ we have elliptic characteristic curves, and for $b^2 = ac$ the curves are parabolic.

These correspond to three different physical phenomena described by different kinds of equations. The hyperbolic case corresponds to the D'Alamberts wave equation, the elliptic case to the Laplace equation, and the parabolic one to the diffusion equation. This way the three-dimensional parameter space of vectors (a, b, c) is partitioned according to the function D.

6.2 Second order stochastic partial differential equations

Let us consider stochastic second order PDE's of one spatial and time coordinate of the form

$$\alpha_1 \frac{\partial h}{\partial t} + \alpha_2 \frac{\partial^2 h}{\partial t^2} + \alpha_3 \left(\frac{\partial h}{\partial t} \right)^2 = \beta_1 \frac{\partial h}{\partial x} + \beta_2 \frac{\partial^2 h}{\partial x^2} + \beta_3 \left(\frac{\partial h}{\partial x} \right)^2 + \eta, \qquad (6.3)$$

where the parameters $(\alpha_1, \alpha_2, \alpha_3, \beta_1, \beta_2, \beta_3)$ are real-valued and η denotes the noise. With a given noise we do not need additional parameters to describe it so that each model is a vector of the six-dimensional parameter space. Examples of such equations [81, 82, 83] include the random deposition model (RD), the Edwards-Wilkinson equation (EW) and the Kardar-Parisi-Zhang equation (KPZ), and the stochastic version of telegrapher equation (STG), for which the coefficients are commonly written as

$(\alpha_1, \alpha_2, \alpha_3, \beta_1, \beta_2, \beta_3)$	model
(1,0,0,0,0,0)	RD
(1,0,0,0,ν,0)	EW
(1,0,0,0,ν,$\lambda/2$)	KPZ
(1,τ,0,ν,0)	STG

The Maxwell equations are invariant under Lorentz transformations, which means that their form does not change if the Lorentz transformation is applied to coordinates. The wave equation is a Lorentz invariant equation, but because of their diffusive nature, the EW equation and the KPZ equations are not. Such equations are often analysed by scaling approach, where the coordinates are transformed by scaling. Usually, linear scaling does not work but the coordinates have to be transformed by using a power law scaling [81, 84].

Consider next the stochastic process given by the vector $(0, \frac{\nu}{c^2}, \frac{\lambda}{2c^2}, 0, \nu, \lambda/2)$. The parameters are here labeled to suggest a formal connection with the 1+1-

dimensional KPZ equation

$$\frac{\partial h}{\partial t} = \nu \frac{\partial^2 h}{\partial x^2} + \frac{\lambda}{2}\left(\frac{\partial h}{\partial x}\right)^2 + \eta(x,t), \tag{6.4}$$

where we now assume "annealed" noise $\eta = \eta(x,t)$ with the correlator

$$\langle \eta(x_1,t_1), \eta(x_2,t_2)\rangle = \delta(x_1 - x_2)\delta(t_1 - t_2). \tag{6.5}$$

The Lorentz transformation in 1+1 dimensionsis is defined by $x' = \gamma(x - vt)$, $t' = \gamma(t - vx/c^2)$, where $\gamma = 1/\sqrt{1-(v/c)^2}$, and c is the speed of light. It transforms equations of motion from a rest frame to a frame moving with velocity v. The KPZ equation is naturally not Lorentz invariant, which can be immediately seen by substituting the Lorentz transformation, which results in

$$\begin{aligned}\gamma\left(\frac{\partial h}{\partial t'} - v\frac{\partial h}{\partial x'}\right) &= \gamma^2\nu\left(\frac{\partial^2 h}{\partial x'^2} - \frac{2v}{c^2}\frac{\partial^2 h}{\partial x'\partial t'} + \frac{v^2}{c^4}\frac{\partial^2 h}{\partial x'^2}\right)\\ &+\gamma^2\frac{\lambda}{2}\left(\frac{\partial h}{\partial x'} - \frac{v}{c^2}\frac{\partial h}{\partial t'}\right)^2 + \eta(\gamma(x'+vt'),\gamma(t'+vx'/c^2)).\end{aligned} \tag{6.6}$$

By including only the terms not breaking the Lorentz invariance, and with the coefficients suitably redefined, we obtain a new equation

$$\frac{\nu}{c^2}\frac{\partial^2 h}{\partial t^2} = \nu\frac{\partial^2 h}{\partial x^2} + \frac{\lambda}{2}\left(-\frac{1}{c^2}\frac{\partial h}{\partial t}\right)^2 + \frac{\lambda}{2}\left(\frac{\partial h}{\partial x}\right)^2 + \eta. \tag{6.7}$$

The Lorentz invariance of this equation follows directly from the form of the deterministic part and the invariance of the noise correlator (6.5) as shown in Paper [VII]. In some sense, this equation is a Lorentz invariant counterpart of the KPZ equation. In higher dimensions it becomes

$$\frac{\nu}{c^2}\frac{\partial^2 h}{\partial t^2} = \nu\nabla^2 h + \frac{\lambda}{2}\left[(\nabla h)^2 - \frac{1}{c^2}\left(\frac{\partial h}{\partial t}\right)^2\right] + \eta', \tag{6.8}$$

which we call the noisy nonlinear wave equation (NNW). By applying simple scaling $x \to bx, h \to b^\alpha h, t \to t^z t$ we obtain

$$\frac{\nu}{c^2}\frac{\partial^2 h}{\partial t^2} = b^{2z-2}\nu\nabla^2 h + \frac{\lambda}{2}\left[b^{\alpha-2+2z}(\nabla h)^2 - b^\alpha\frac{1}{c^2}\left(\frac{\partial h}{\partial t}\right)^2\right] + b^{-d/2-3z/2-\alpha}\eta', \tag{6.9}$$

where d is the dimensionality of space. This means that NNW is trivially scale invariant in 3+1 dimensions, i.e. in conventional space-time, with $z = 1$ and $\alpha = 0$.

Chapter 7

Discussion

This Thesis constitutes a review of theoretical ideas and methods that can be applied when dealing with complex parametrised systems, in particular those described by partial differential equations. The goal was to gain insight in the general features and behaviour of such systems. The presented methods emphasise the parameterisation of problems and the subsequent classification of observed behaviour. Classification of data has been widely studied, e.g. in the contexts of pattern recognition, data mining, learning problems, etc. Instead of concentrating on the data itself, we look at the effects due to initial conditions as well. We presented a theoretical framework together with the associated machinery and demonstrated how it can be used to reveal and visualise the systems of quantities of intrest. These include both parameters and measurable physical quantities. These concepts and the method have evolved and they are still under development. First, the idea of partitioning the parameter space was introduced. Simultaneously, the visulisation graphs, also under the name of implementation simplicial complex, were developed in order to consider the dynamics and stability of partitionings. To this end, similarity measures, in the form of matrices, were also used. These tools have been applied mainly to EMC problems such as shielding properties of enclosures. As an extension to the basic method, electric field histograms were introduced to gain further understanding of the origin of the partitionings.

The practical examples considered dealt with data on electromagnetic fields and our methodology works well with that kind of data. Our partitionings into classes were constructed by using chosen mom functions. In order to compare partitionings obtained for different mom values, we introduced two correlation quantities. In our approach, we consider the simulation, both its input and

output, and construct simulation state vectors in terms of the class weights and "convergence" matrices.

We proceeded by studying the stability of the partitioning with respect to the implementation. The dynamics and the stability of the partitioning are visualised by comparing the classes between successive implementations. For two-dimensional parameter spaces, the stabilisation of the partitioning can be depicted directly on the parameter space. In the general case, a practical visualisation requires a projection of the parameter space. The stability of the partitioning with respect to the implementation is estimated using of λ-matrices, that link different implementations.

We demonstrated the applicability of the methodology in FEM simulations. Our case studies consisted of one filter study and several examples of determination of shielding effectiveness of rectangular enclosures. We found that the parameter space description of the selected examples is useful. Some kind of parameter space descriptions can be found in the literature without really taking advantage of their power in visualising the systematics. We also considered simple electric field amplitude histograms and their problem-specific modifications and compared them using suitably defined distance measures. The histograms are classified into groups and the groupings are compared with groupings obtained directly from the shielding effectiveness. The histogram study was also motivated by the fact that practical enclosures are not always electrically large. If the enclosures were bigger (electrically large), we could use the statistical approach to calculate electric field behaviour inside the cavity. A lot of work is still required to fully understand the behaviour of the electric field inside rectangular enclosures with different kinds of apertures.

The final chapter of this Thesis was devoted to the concept of partitioning in the context of more general mathematical models in physics. Particularly, we considered families of second order partial differential and stochastic partial differential equations. Within the parametrisation approach, a possible new process described by a noisy nonlinear wave equation, was identified.

To conclude, in this Thesis various theoretical concepts and links were utilised to introduce methods to analyse practical problems described by parametrised models. This area of research is very active and new ideas appear constantly. Further development and extensions of the presented methods should prove useful.

Bibliography

[I] J. S. Hämäläinen, H. J. Rajaniemi and K. P. Hirvi, *Using mathematical models to cope with complex computer simulations*, IEEE Computing in Science and Engineering, Vol. 4, No. 1, 2002, pp. 64-72.

[II] J. S. Hämäläinen, P. S. Järviö and S. R. Malm, *Novel description of a numerical EMC problem*, Proceedings of EMC Europe 2002, 9–13 September 2002, Sorrento, Italy, pp. 591-594.

[III] J. S. Hämäläinen, M. Aunola and S. R. Malm, *Exploring the overall behaviour of solutions of recursive computational models*, to appear in COMPEL, The International Journal for Computation and Mathematics in Electrical and Electronic Engineering, 2005.

[IV] S. R. Malm and J. S. Hämäläinen, *Grouping the distributions of electric field amplitudes*, Proceedings of the 2003 IEEE International Symposium on Electromagnetic Compatibility, Istanbul, 2003.

[V] S. R. Malm, J. S. Hämäläinen and S. A. Helle, *Determination the optimal measurement parameters from simulations*, in Electrical engineering and electromagnetics VI, edited by C. A. Brebbia and D. Poljak, WIT Press, 2003, pp. 293-302.

[VI] J. S. Hämäläinen, *Are shielding properties of the cavity readable in histograms of electric field amplitudes - to scale or not to scale histograms*, to appear in IEE Proceedings - Science, Measurement and Technology, 2004.

[VII] J. S. Hämäläinen and J. Merikoski, *Stochastic kinetics with wave nature*, Modern Physics Letters B, Vol. 17, No. 17, 2003, pp. 929-933.

[1] C. M. Bishop, *Neural Networks for Pattern Recognition*, Oxford University Press, New York, 1995.

[2] R. O. Duda, P. E. Hart and D. G. Stork, *Pattern Classification*, John Wiley & Sons, Inc., New York, 2001.

[3] T. Kohonen, *Self-Organizing Maps*, Springer, Berling/Heidelberg, Germany, 1995.

[4] Eds. J. C. Bezdek and S. K. Pal, *Fuzzy Models for Pattern Recognition: Methods that Search for Structures in Data*, IEEE, New York, 1992.

[5] M. Pardo and G. Sberveglieri, *Learning From Data: A Tutorial With Emphasis on Modern Pattern Recognition Methods*, IEEE Sensors Journal, Vol. 2, No. 3, 2002, pp. 203-217.

[6] J. Daintith and R. D. Nelson, *Dictionary of Mathematics*, Penguin Books, 1989.

[7] J. Vesanto and E. Alhoniemi, *Clustering of the self-organizing map*, IEEE Transactions on Neural Networks, Vol. 11, No. 3, 2000, pp. 586-600.

[8] C. Traina Jr., et al., *Fast Indexing and Visualization of Metric Data Sets Using Slim-Trees*, IEEE Transactions on Knowledge and Data Engineering, Vol. 14. No. 2, 2002, pp. 244-260.

[9] J. S. Hämäläinen, *Analogy between 'convergence' and comparison of different data groupings*, Proceedings of the European Congress on Computational Methods in Applied Sciences and Engineeering ECCOMAS 2004, Jyväskylä, 2004.

[10] D. M. Butler and S. Bryson, *Vector-bundle classes form powerful tool for scientific visualization*, Computers in Physics, Vol. 6, No. 6, 1992, pp. 576-584.

[11] D. M. Butler and M.H. Pendley, *A Visualization model based on the mathematics of fiber bundles*, Computers in Physics, Vol. 3, No. 5, 1989, pp. 45-51.

[12] H. Edelsbrunner and E. P. Mücke, *Three-dimensional alpha shapes*, ACM Transactions on Graphics, Vol. 13, No. 1, 1994, pp. 43-72.

[13] E. Mücke, *Shapes and Implementations in Three-dimensional Geometry*, Ph.D. Thesis, University of Illinois at Urbana-Champaign, 1993.

[14] W. Wang, J. Yang and R. Muntz, *An Approach to Active Spatial Data Mining Based on Statistical Information*, IEEE Transactions on Knowledge and Data Engineering, Vol. 12, No. 5, 2000, pp. 715-728.

[15] M. R. Anderberg, *Cluster Analysis for Applications*, Academic Press, New York, 1973.

[16] K. Hirvi, S. Malm and J. Hämäläinen, *Using Matlab as a Control Center for Third Party Simulation Software*, Proceedings of the Nordic Matlab Conference 2001, Oslo, Norway, pp. 182-185.

[17] D. White and M. Mardiguian, *Electromagnetic Shielding (Electromagnetic Interference and Compatibility Series, Vol. 3*, Interference Control Technologies, Inc., 1988.

[18] M. S. Sarto et al., *Nanotechnology of Transparent Metals for Radio Frequency Electromagnetic Shielding*, IEEE Transactions on Electromagnetic Compatibility, Vol. 45, No. 4, 2003, pp. 586-594.

[19] MIL-STD 285, *Method of Attenuation Measurements for Enclosures, Electromagnetic Shielding for Electronic Test Purposes*, U. S. Goverment Printing Office, Washington, DC, 1956.

[20] IEEE-STD 299, *Standard Method for Measuring the Effectiveness of Electromagnetic Shielding Enclosures*, IEEE, Piscataway, NJ, 1991.

[21] ASTM E1851-97, *A Test Procedure to Evaluate Shielding Effectiveness of a Shielded Enclosure*, ASTM, West Conshohocken, PA, 1997.

[22] L. T. Gnecco, *The Design of Shielded Enclosure Cost-Effective Methods to Prevent EMI*, Newnes, Boston, USA, 2000.

[23] I. Belekour, J. LoVetri and S. Kashyap, *A Higher-order transmission line model of the shielding effectiveness of enclosures with apertures*, Proceedings of IEEE EMC International Symposium, Montreal, 2001, pp. 702-707.

[24] V. Trenkić, C. Cristopaulos and T. M Benson, *Simulation of the shielding effectiveness of cabinets used in communications equipment*, Facta Universitatis (NIS), Series: Electronics and Energetics Vol. 9, No. 1, 1996, pp. 13-19.

[25] J. E. Bridges, *An Update on the circuit approach to calculate shielding effectiveness*, IEEE Transactions on Electromagnetic Compatibility, Vol. 30. No. 3, 1998, pp. 211-221.

[26] M. P. Robinson et al., *Shielding effectiveness of a reactangular enclosure with a rectangular aperture*, Electronics Letters, Vol. 32 No. 17, 1996, pp. 1559-1560.

[27] IEEE Std 145-1993, *IEEE Standard Definitions of Terms for Antennas*, IEEE, New York, USA, 1993.

[28] H. A. Bethe, *Theory of diffraction of small holes*, Physical Review, 2nd series, Vol. 66, No. 7-8, 1944, pp. 163-182.

[29] T. Martin, M. Bäckström and J. Lorén, *Semi-Empirical Modeling of Apertures for Shielding Effectiveness Simulations*, IEEE Transactions on Electromagnetic Compatibility, Vol. 45, No. 2, 2003, pp. 229-237.

[30] W. Wallyn, D. De Zutter and E. Laermans, *Fast Shielding Effectiveness Prediction for Realistic Rectangular Enclosures*, IEEE Transactions on Electromagnetic Compatibility, Vol. 45, No. 4, 2003, pp. 639-643.

[31] R. Holland and R. St. John, *Statistical Electromagnetics*, Taylor & Francis, Philadelphia, 1999.

[32] R. Holland and R. H. St. John, *Statistical responce of EM-driven cables inside an overmoded enclosure*, IEEE Transactions on Electromagnetic Compatibility, Vol. 40, No. 4, 1998, pp. 311-324.

[33] F. Ustuner et al., *A Method for evaluating shielding effectiveness of small enclosure*, Proceedings of IEEE EMC International Symposium, Montreal, 2001, pp. 708-712.

[34] H. A. Méndez, *Shielding theory of enclosures with apertures*, IEEE Transactions on Electromagnetic Compatibility, Vol. EMC-20, No. 2, 1978, pp. 296-305.

[35] A. Taflove and S. C. Hagness, *Computational Electrodynamics: The Finite Difference Time-Domain Method*, 2nd *Edition*, Artech House, Inc., Boston, 2000.

[36] R. Banncroft, *Understanding Electromagnetic Scattering Using the Moment Method, A Practical Approach*, Artech House, Inc., Boston, 1996.

[37] J. Jin, *The Finite Element Method in Electromagnetics*, John Wiley & Sons, New York, 1993.

[38] T. Rylander and A. Bondeson, *Stable FEM-FDTD method for Maxwell's equations*, Computer Physics Communications, Vol. 125, 2000, pp. 75-82.

[39] G. Caccavo et al., *ESD field penetration into populated metallic enclosure: a hybrid time domain approach*, IEEE Transactions on Electromagnetic Compatibility, Vol. 44, No. 1, 2002, pp. 243-249.

[40] K-P. Ma et al., *Comparison of FDTD algorithms for subcellular modelling of slots in shielded enclosures*, IEEE Transactions on Electromagnetic Compatibility, Vol. 39, No. 2, 1997, pp. 147-155.

[41] W. Wallyn et al., *A new efficient formulation for modelling the shielding effectiveness of metallic enclosures*, Proceedings of 14th International Zürich Symposium and Technical Exhibition on Electromagnetic Compatibility, Zürich, 2001, pp. 1-4.

[42] I. Belekour, J. LoVetri and S. Kashyap, *Shielding effectiveness estimation of enclosures with apertures*, Proceedings of IEEE Electromagnetic Compatibility Symposium, Washington, 2000, pp. 855-860.

[43] F. M Tesche, M. V Ianoz and T. Karlsson, *EMC Analysis Methods and Computational Models*, John Wiley & Sons, Inc., New York, 1997.

[44] M. M. Ney, *Electromagnetic modeling in EMC*, Proceedings of 14th International Zürich Symposium and Technical Exhibition on Electromagnetic Compatibility, Zürich, 2001, pp. 385-388.

[45] B. Audone and M. Palma, *Shielding effectiveness of apertures in rectangular cavities*, IEEE Transactions on Electromagnetic Compatibility, Vol. 31, No. 1, 1989, pp. 102-106.

[46] M. P. Robinson et al., *Analytic formulation for the shielding effectiveness of enclosures with apertures* IEEE Transactions on Electromagnetic Compatibility, Vol. 40, 1998, No. 3, pp. 240-248.

[47] H. H. Park and H. J. Enom, *Electromagnetic penetration into a rectangular cavity with multiple rectangular apertures in a conducting plane*, IEEE Transactions on Electromagnetic Compatibility, Vol. 42, No. 3, 2000, pp. 303-307.

[48] T. I. Williams, *EMC for Product Designers Meeting the European EMC Directive*, Newnes, Oxford, 1999.

[49] S. Dey and R. Mittra, *Efficient computation of resonant frequencies and quality factors of cavities via a combination of the finite-difference time-domain technique and the Padé Approximation*, IEEE Microwave and Guided Wave Letters, Vol. 8, No. 12, 1998, pp. 415-417.

[50] S. Primak and J. LoVetri, *The Search for a Statistical Approach Capable of Predicting the Coupling Strength from an External Electromagnetic*

Field to Electronic Equipment, Technical Report for University of Western Ontario and CRC, Ottawa, Canada, 1999.

[51] R. H. Price, H. T. Davis and E. P. Wenaas, *Determination of the statistical distribution of electromagnetic-field amplitudes in complex cavities*, Physical Review E, Vol. 48, No. 6, 1993, pp. 4716-4729.

[52] F. Olyslager et al., *Numerical and experimental study of shielding effectiveness of a metallic enclosure*, IEEE Transactions on Electromagnetic Compatibility, Vol. 41, No. 3, 1999, pp. 202-213.

[53] D. W. P. Thomas et al., *Model of the electromagnetic fields inside a cuboidal enclosure populated with conducting planes or printed circuit boards*, IEEE Transactions on Electromagnetic Compatibility, Vol. 43, No. 2, 2001, pp. 161-169.

[54] W. Wallyn and D. De Zutter., *Modeling the shielding effectiveness of metallic shielding enclosures loaded with PCB's*, Proceedings of IEEE EMC International Symposium, Montreal, 2001, pp. 691-696.

[55] D. A. Hill et al., *Aperture excitation of electrically large lossy cavities*, IEEE Transactions on Electromagnetic Compatibility, Vol. 36, No. 3, 1994, pp. 169-178.

[56] D. Taylor and D. V. Giri, *High-Power Microwave Systems and Effects*, Taylor & Francis, Washington, 1994.

[57] S. Celozzi, *New figures of merit for characterization of the performance of shielding enclosures*, IEEE Transactions on Electromagnetic Compatibility, Vol. 46, No. 1, 2004, p. 142.

[58] L. D. Landau and E. M. Lifshitz, *Statistical Physics, Part 1,* 3rd *Edition*, Butterworth-Heinemann, Oxford, 1999.

[59] L. D. Landau and E. M. Lifshitz, *Electrodynamics of Continous Media,* 2nd *Edition*, Butterworth-Heinemann, Oxford, 1999.

[60] T. H. Lehmann, *The Statistics of Electromagnetic Fields in Cavities with Complex Shapes*, Phillips Laboratory, Albuquerque, NM, Interaction Note 494, 1993.

[61] M. Bäckström, T. Martin and J. Lorén, *Analytical model for bounding estimates of shielding effectiveness of complex resonant cavities*, Proceedings

of the 2003 IEEE International Symposium on Electromagnetic Compatibility, Istanbul, 2003.

[62] M. Bäckström, O. Lundén and P.-S. Kildal, *Rewiev of Radio Science 1999-2002*, in Chapter 18, Wiley-Interscience, John Wiley & Sons, Inc., New York, 2002.

[63] D. A. Hill, *Electronic mode stirring for reverberation chambers*, IEEE Transactions on Electromagnetic Compatibility, Vol. 36, No. 4, 1994, pp. 294-299.

[64] D. A. Hill, *Plane wave integral representation for fields in reverberation chambers*, IEEE Transactions on Electromagnetic Compatibility, Vol. 40, No. 3, 1998, pp. 209-217.

[65] K. Rosengren and P.-S. Kildal, *Theoretical study of angular distribution of plane waves in a small reverberation chamber for simulating multipath environment and testing mobile phones*, Proceedings of the Antennas and Propagation Society, 2001 IEEE International Symposium, Vol. 3, 2001, pp. 358-361.

[66] D. A. Hill, *Spatial correlation function for fields in a reverberation chamber*, IEEE Transactions on Electromagnetic Compatibility, Vol. 37, No. 1, 1995, p. 138.

[67] D. A. Hill and J. M. Ladbury, *Spatial-correlation functions of fields and energy density in a reverberation chamber*, IEEE Transactions on Electromagnetic Compatibility, Vol. 44, No. 1, 2002, pp. 95-101.

[68] S. Primak, J. LoVetri and J. Roy, *On the statistics of a sum of harmonic waveforms*, IEEE Transactions on Electromagnetic Compatibility, Vol. 44, No. 1, 2002, pp. 266-271.

[69] L. R. Arnaut, *Statistics of the quality factor of a rectangular reverberation chamber*, IEEE Transactions on Electromagnetic Compatibility, Vol. 45, No. 1, 2003, pp. 61-76.

[70] L. R. Arnaut, *Limit distributions for imperfect electromagnetic reverberation*, IEEE Transactions on Electromagnetic Compatibility, Vol. 45, No. 2, 2003, pp. 357-377.

[71] C. F. Bunting et al., *A two-dimensional finite-element analysis of reverberation chambers*, IEEE Transactions on Electromagnetic Compatibility, Vol. 41, No. 4, 1999, pp. 280-289.

[72] C. F. Bunting, *Statistical characterization and the simulation of a reverberation chamber using finite-element techniques*, IEEE Transactions on Electromagnetic Compatibility, Vol. 44, No. 1, 2002, pp. 214-221.

[73] C. F. Bunting, *Shielding effectiveness in a two-dimensional reverberation chamber using finite-element techniques*, IEEE Transactions on Electromagnetic Compatibility, Vol. 45, No. 3, 2003, pp. 548-552.

[74] G. J. Freyer et al., *Comparison of measured and theoretical statistical parameters of complex cavities*, Proceedings of IEEE 1996 International Symposium on Electromagnetic Compatibility, August 1996, pp. 250-253.

[75] S. Silfverskiöld, M. Bäckström and J. Lorén, *Microwave field-to-wire coupling measurements in anechoic and reverberation chambers*, IEEE Transactions on Electromagnetic Compatibility, Vol. 44, No. 1, 2002, pp. 222-232.

[76] P. Huuhtanen, *Stochastic Complexity and the MDL Principle in Density Function Estimation*, Ph. D. Thesis, University of Tampere, Tampere, 1998.

[77] D. W. Scott, *On optimal and data-based histograms*, Biometrika, Vol. 66, No. 3, 1979, pp. 605-610.

[78] I. L. Dryden and K. V. Mardia, *Statistical Shape Analysis*, John Wiley & Sons, Great Britain, Chichester, 2002.

[79] J. B. Westgard, *Electrodynamics: A Concise Introduction*, Springer-Verlag, 1997.

[80] J. Ockendon, S. Hawison, A. Lacey and A. Movchan, *Applied Partial Differential Equations*, Oxford University Press, 1999.

[81] A.-L. Barabasi and H. E. Stanley, *Fractal Concepts in Surface Growth*, Cambridge University Press, Cambridge, 1995.

[82] S. F. Edwards and D. R. Wilkinson, *The surface statistics of a granular aggregate*, Proceedings of the Royal Society, London, Vol. A381, 1982, pp. 17-31.

[83] M. Kardar, G. Parisi and Y-L. Zhang, *Dynamical scaling of growing interfaces*, Physical Review Letters, Vol. 56, No. 9, 1986, pp. 889-892.

[84] G. I. Barenblatt, *Scaling, Self-similarity and Intermediate Asymptotics*, Cambridge University Press, Cambridge, 1996.